Finite orbital-angular-momentum carried by the final electron and photon in plane-wave electron-nucleus bremsstrahlung

Weiqing Wang,[1,2] Shiyu Liu,[1,2] Shaohu Lei,[1,2] Xuesong Geng,[1] Baifei Shen,[3] Zhigang Bu,[1,*] and Liangliang Ji[1,4,†]

[1]*State Key Laboratory of High Field Laser Physics, Shanghai Institute of Optics and Fine Mechanics, Chinese Academy of Sciences, Shanghai 201800, China*

[2]*Center of Materials Science and Optoelectronics Engineering, University of Chinese Academy of Sciences, Beijing 100049, China*

[3]*Shanghai Normal University, Shanghai 200234, China*

[4]*CAS Center for Excellence in Ultra-intense Laser Science, Shanghai 201800, China*

(Received 11 February 2022; accepted 4 April 2022; published 2 May 2022)

In quantum-electrodynamics scatterings the transfer of angular momentum between initial and final states can be resolved using the vortex scattering theory, where involved particles are described by quantum vortex states with featured orbital angular momentum (OAM). Here we employ the vortex scattering scenario in bremsstrahlung of a plane-wave electron by describing the final electron and photon in vortex states. We find that, while the total cross-section and angular distribution of the vortex scattering scenario are consistent with those from the ordinary plane-wave scattering, the final states in the former can gain non-negligible OAM values even though the incident electron does not contain any OAM. Moreover, introducing the OAM degree of freedom conserves the total angular momentum in polarized scattering. The dependence of the OAM on the opening angle of the vortex state and the energy ratio of photon to electron are obtained. It is shown that the emitted photon gains higher OAM at larger angles and energy ratios.

DOI: 10.1103/PhysRevResearch.4.023084

I. INTRODUCTION

In quantum field theory, particle scattering processes are usually interpreted by use of plane wave (PW) states as the complete basis for field quantization. This theoretical framework is extremely successful when energy and momentum of the involved particles are the main focus. It also allows for analysis of the spin-polarization properties during the interaction [1]. However, since the PW states do not contain intrinsic orbital-angular-momentum (OAM) information, it is in principle not capable of describing the angular-momentum (AM) of particles. In fact, spin-orbital coupling or the transfer of OAM often exists in a large group of scattering processes, especially when the initial particles are spin polarized. Such problems cannot be fully resolved in the PW scattering framework. Instead, one may switch to the basis that carry definite quantum numbers of AM to obtain the scattering probabilities or cross sections.

In 1992, optical photons with distinctive OAM numbers were proposed (referred as vortex or twisted photon) in theory [2] and later experimentally confirmed [3,4]. Subsequently, low-energy vortex or twisted electron states with OAM have also been experimentally generated and applied to transmission electron microscopy (TEMs) [5–7]. These vortex light wave or particles provide the OAM degree of freedom in manipulating light-matter interaction [8,9] as well as increasing the signal-background ratio in probing the material properties [6].

In the high-energy regime, it is pointed out theoretically that particles described in the quantum vortex states take certain OAM [10–12]. The role of angular momentum in high-energy inelastic scattering is studied in various processes [13–28]. The new effects of vortex states are studied by changing the description of one or several particles in the scattering process from plane-wave states to vortex states, such as the difference between paraxial and nonparaxial cases [29,30], scattering described by wave packets [31], study of coherence length effect in collision [32], nonlinear quantum effect of vortex electrons electromagnetic radiation [33], the Vavilov-Cherenkov radiation emitted by twisted electrons [34], observation of Larmor and Gouy rotation by vortex electrons beam [35], vortex electrons characteristics under external magnetic field [36], and some other effects [37,38].

In this paper, to reveal the effect of angular momentum existing in QED scattering, we calculate the differential cross section of the bremsstrahlung for a PW electron colliding with a lead nucleus. We describe the final electron and photon in vortex states, i.e., PW+nucleus→V+V (P-V bremsstrahlung) and compare the differential cross section to the one from the normal treatment where all particles are described by PW states PW+nucleus→PW+PW (PW bremsstrahlung). The angular distribution of the outgoing electron and photon is analyzed. By studying the OAM distribution of the scattered

*zhigang.bu@siom.ac.cn
†jill@siom.ac.cn

particles, we find that they gain non-negligible OAM values even though the initial electron does not have any OAM. It originates from the AM transferred from electron spin angular momentum (SAM) to OAM such that the total AM is conserved. The scalings as a function of different photon energy ratios are further discussed.

II. THEORETICAL BACKGROUND OF THE VORTEX STATE

The scalar electron wave function without spin satisfies the Schrödinger equation. We discuss the scattering of high-energy electrons and study the spin related properties, which require that the electrons be treated in a fully relativistic manner. Therefore, the electron state follows the solution of the free Dirac equation $(i\partial\!\!\!/ - M)\psi = 0$, expressed in spinors.

The plane-wave function then takes the form of Eq. (1), where E is energy and M is the rest mass of electrons. $\boldsymbol{\sigma}$ is the Pauli matrix. The unit momentum vector is defined as $\boldsymbol{\kappa} = \vec{p}/|\vec{p}|$. ξ^s ($s = \pm 1$ is the spin projection on the momentum direction z-axis, called helicity usually) represent the two-component basis spinors, such as

$$\begin{bmatrix}1\\0\end{bmatrix}, \quad \begin{bmatrix}0\\1\end{bmatrix},$$

which are orthogonal. In this paper, the relativistic units $c = \hbar = 1$ are used. When PW states are used to describe the scattering processes, helicity is usually introduced to distinguish polarization scattering [1]. However, because the PW states do not contain OAM information, the discussion of angular-momentum transfer or conservation of polarization scattering becomes difficult.

$$\psi_p^s(x) = \frac{1}{\sqrt{2(2\pi)^3}} e^{-ipx}\left(\sqrt{1+\frac{M}{E}}\xi^s, \sqrt{1-\frac{M}{E}}(\boldsymbol{\sigma}\cdot\boldsymbol{\kappa})\xi^s\right). \tag{1}$$

Vortex states were later introduced as another exact solution of Dirac equation [25,39]. The vortex structure can be formed by the superposition of plane-wave states in the momentum direction perpendicular to the z axis of the propagation direction: $\psi_m^s(x) = \int \tilde{\psi}_m(\vec{p'}_\perp)\psi(x)p'_\perp dp'_\perp d\phi$, where $\tilde{\psi}_m(p'_\perp) = \frac{1}{\sqrt{2\pi}i^m p'_\perp}\delta(p'_\perp - p_\perp)e^{im\phi_{p'}}$ is the Fourier spectrum. Due to the axisymmetric property of vortex states, it is usually described in cylindrical coordinate system. The wave function of electron vortex states can be expressed as follows [39]:

$$\begin{aligned}\psi^{m,s}_{p_\perp,p_z}(x) &= u^{m,s}_{p_\perp,p_z}(r,\theta)e^{ip_z z - iEt}\\ &= \frac{e^{ip_z z-iEt}}{\sqrt{2}(2\pi)}\frac{1}{|\vec{p}|}\sqrt{1-\frac{M}{E}}\left[\begin{pmatrix}(E+M)\xi^s\\ p_z\sigma_z\xi^s\end{pmatrix}\Theta^m_{p_\perp}(r)\right.\\ &\quad \left. + ip_\perp\begin{pmatrix}0\\ \sigma^{\perp,m}_{p_\perp}(r,\theta)\xi^s\end{pmatrix}\right].\end{aligned} \tag{2}$$

Here p_z and $p_\perp = (E^2 - M^2 - p_z^2)^{1/2}$ are the z component and perpendicular one of the electron momentum. The transversal matrix reads

$$\sigma^{\perp,m}_{p_\perp}(r,\theta) = \begin{bmatrix}0 & -\Theta^{m-1}_{p_\perp}(r)\\ \Theta^{m+1}_{p_\perp}(r) & 0\end{bmatrix}.$$

Similarly, we construct the photon vortex states by employing the Bessel mode $A^{j,\lambda;\mu}_{k_\perp,k_z}(x) = \int \tilde{A}_j(k'_\perp)A^{\lambda;\mu}_{k'_\perp,k_z}(x)k'_\perp dk'_\perp d\phi_{k'}$. Suppose that the vortex photon propagates along the z axis, j and $\lambda = \pm 1$ are the projections of total angular momentum (TAM) and spin on momentum direction z axis (we call it TAM and helicity to simplify), respectively. k_z and $k_\perp = (\omega^2 - k_z^2)^{1/2}$ (ω is the photon energy) are the photon momentum parallel and perpendicular the z axis, respectively. Here

$$A^{\lambda;\mu}_k(x) = \frac{\epsilon^{\lambda;\mu}_k}{[(2\pi)^3(2\omega)]^{1/2}}e^{-ikx}$$

is the PW photon states, $\tilde{A}_j(k'_\perp) = \frac{1}{\sqrt{2\pi}i^j k'_\perp}\delta(k'_\perp - k_\perp)e^{ij\phi_{k'}}$ is the corresponding Fourier spectrum. So, the vortex photon states can be expressed as [39]

$$\begin{aligned}&A^{j,\lambda;\mu}_{k_\perp,k_z}(x)\\ &= \epsilon^{j,\lambda;\mu}_{k_\perp,k_z}(\vec{r}\,)e^{ik_z z - i\omega t}\\ &= \frac{e^{ik_z z-i\omega t}}{4\pi\sqrt{\omega}}\begin{pmatrix}0\\ \left(\frac{i}{2}\right)\left[\left(1-\frac{k_z}{\omega}\right)\Theta^{j+\lambda}_{k_\perp}(\vec{r}\,)+\left(1+\frac{k_z}{\omega}\right)\Theta^{j-\lambda}_{k_\perp}(\vec{r}\,)\right]\\ \left(\frac{\lambda}{2}\right)\left[\left(1-\frac{k_z}{\omega}\right)\Theta^{j+\lambda}_{k_\perp}(\vec{r}\,)-\left(1+\frac{k_z}{\omega}\right)\Theta^{j-\lambda}_{k_\perp}(\vec{r}\,)\right]\\ \left(\frac{\lambda k_\perp}{\omega}\right)\Theta^{j}_{k_\perp}(\vec{r}\,)\end{pmatrix},\end{aligned} \tag{3}$$

where $\epsilon^{l,\lambda;\mu}_{k_\perp,k_z}(\vec{r}\,)$ represents the polarization vector and the transverse function is defined by $\Theta^n_{k_\perp}(\vec{r}\,) = J_n(k_\perp r)e^{in\theta}$ [$J_n(r)$ is the first kind of Bessel function]. Equations (2) and (3) contain intrinsic OAM information and thus can be employed in resolving the AM-related physics in various scattering processes.

Here we define a quantity $l = j - \lambda$ for the vortex photon. It corresponds to the OAM projection number of photon on z axis in a paraxial approximation, where j and λ represent the TAM and spin projection of photon on the z axis. One should notice that m and l are not the eigenvalues of the OAM operator $\hat{L}$, but usually referred as OAM projection of electron and photon on the z axis [10,20,28–31,35,40–42]. It is clear that only $s/2 + m$ and $\lambda + l$ are the eigenvalues of the corresponding operators of vortex electron and photon states, respectively.

III. THE DIFFERENTIAL CROSS SECTION OF THE P-V BREMSSTRAHLUNG

We assume that a PW electron propagates along the z axis. After colliding with a stationary bare lead nucleus, the outgoing electron and emitted photon are scattered forward defined by the vortex states along the z axis, as illustrated in Fig. 1(a). For comparison, Fig. 1(b) shows the process of PW bremsstrahlung.

The S-matrix element of P-V bremsstrahlung can be written as in the QED framework:

$$\begin{aligned}S_{fi} &= S_1 + S_2\\ &= -ie^2\int d^4x d^4y \overline{\psi_f}(x)[\gamma^0 A_0(x)S_F(x-y)\gamma^\nu A^*_\nu(y)\\ &\quad + \gamma^\mu A^*_\mu(x)S_F(x-y)\gamma^0 A_0(y)]\psi_i(y),\end{aligned} \tag{4}$$

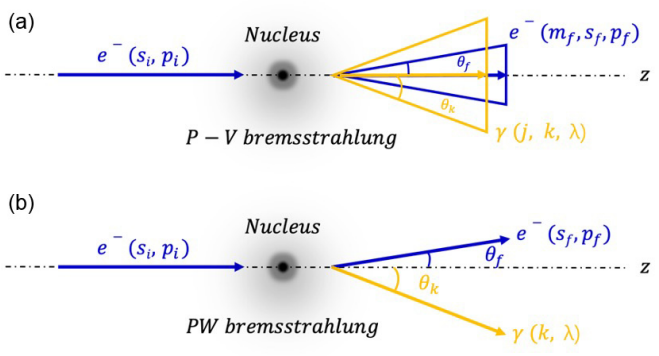

FIG. 1. Kinematics of P-V and PW bremsstrahlung.

where $\psi_i(y)$ represents the wave function of the incident PW electron and $\psi_f(x)$ represents the wave function of the outgoing vortex electron. The electron propagator is defined as $S_F(x-y) = \int \frac{d^4p}{(2\pi)^4} \frac{\gamma_\mu p^\mu + M}{p^2 - M^2} e^{-ip(x-y)}$ and $A_0 = -\frac{Ze}{4\pi|\vec{x}|}$ is the Coulomb field of the nucleus (for a lead nucleus, $Z = 82$).

Combining Eqs. (1)– (4), we obtain

$$S_{\text{P-V}} = \frac{-ize^3}{(4\pi)^2\sqrt{2\pi}}\delta(E_f + \omega - E_i)\frac{\sqrt{(E_f - M)(E_i - M)}}{\sqrt{\omega E_f E_i}} \times \int dq_\perp \frac{q_\perp}{(p^2 - M^2)|\vec{p}_f||\vec{p}_i||\vec{q}\,|^2} \times \xi^{s_f\dagger}(C_1 + C_2)\xi^{s_i}. \quad (5)$$

The derivations are carried out in cylindrical coordinate system because of the axisymmetric nature of vortex states. Matrices C_1 and C_2 have the following forms after calculation (see Appendix A for details):.

$$C_1 = (M_1 + M_2 + M_3 + M_4 + M_5 + M_6)|_{p_z = p_{fz} + k_z, q_z = p_{fz} + k_z - p_{iz}, E_p = E_i, p_\perp = q_\perp}, \quad (6)$$

$$C_2 = (M_1' + M_2' + M_3' + M_4' + M_5' + M_6')|_{p_z = p_{iz} - k_z, E_p = E_f, q_z = p_{fz} - p_{iz} + k_z, p_\perp = k_\perp}. \quad (7)$$

We define matrices Σ_1 and Σ_2:

$$\Sigma_1 = \int dq_\perp q_\perp \frac{1}{(p^2 - M^2)|\vec{q}\,|^2} C_1, \quad (8)$$

$$\Sigma_2 = \int dq_\perp q_\perp \frac{1}{(p^2 - M^2)|\vec{q}\,|^2} C_2. \quad (9)$$

Then,

$$S_{\text{P-V}} = \frac{-iZe^3}{(4\pi)^2\sqrt{2\pi}}\delta(E_f + \omega - E_i)\frac{\sqrt{(E_f - M)(E_i - M)}}{\sqrt{\omega E_f E_i}|\vec{p}_f||\vec{p}_i|} \times \xi^{s_f\dagger}(\Sigma_1 + \Sigma_2)\xi^{s_i}. \quad (10)$$

Matrix $\Sigma_1 + \Sigma_2$ takes the following form:

$$\Sigma_1 + \Sigma_2 = \begin{bmatrix} A\delta_{m_f,-j} & B\delta_{m_f,-j-1} \\ C\delta_{m_f,-j+1} & D\delta_{m_f,-j} \end{bmatrix}, \quad (11)$$

where A, B, C, and D are the coefficients of the four matrix elements (see Appendix A). The four Kronecker symbols represent the TAM conservation corresponding to four spin cases. For example, consider that both the incident and the outgoing electron spins are up:

$$\xi^{s_i} = \begin{bmatrix} 1 \\ 0 \end{bmatrix}, \quad \xi^{s_f} = \begin{bmatrix} 1 \\ 0 \end{bmatrix},$$

the relationship given by the conservation law of TAM is $\frac{1}{2} = (m_f + \frac{1}{2}) + j$, and the corresponding term is $A\delta_{m_f,-j}$.

According to Fermi's golden rule, the scattering cross section of P-V bremsstrahlung is as follows:

$$d\sigma = \frac{|S_{\text{P-V}}|^2\left(\frac{(2\pi)^3}{V}\right)p_{f\perp}k_\perp dp_{f\perp}dp_{fz}dk_\perp dk_z}{T\frac{|\vec{v}_i|}{V}} = \frac{Z^2e^6}{(4\pi)^5\pi}\delta(\omega + E_f - E_i)\frac{(E_f - M)(E_i - M)}{\omega E_f|\vec{p}_f|^2|\vec{p}_i|^3} \times |\xi^{s_f\dagger}(\Sigma_1 + \Sigma_2)\xi^{s_i}|^2 p_{f\perp}k_\perp dp_{f\perp}dp_{fz}dk_\perp dk_z. \quad (12)$$

Comparing with PW states, vortex states not only carry OAM information but also exhibit different momentum-space structure. The angle of the PW particle is the emission angle, while the one for vortex state corresponds to the opening angle composed of z-axis momentum and vertical momentum, e.g., θ_f, θ_k in Fig. 1. Transfer the rectangular coordinate system composed of p_z and $p_\perp$ to the polar coordinate system composed of θ and E via $E^2 = M^2 + p_\perp^2 + p_z^2$ ($\omega^2 = k_\perp^2 + k_z^2$ for a photon), we have $dp_{f\perp}dp_{fz} = E_f dE_f d\theta_f$ and $dk_\perp dk_z = \omega d\omega d\theta_k$, where θ_k and θ_f are the opening angles of outgoing photon and electron following $k_\perp = \omega\sin\theta_k$, $k_z = \omega\cos\theta_k$, $p_{f\perp} = (E_f^2 - M^2)^{1/2}\sin\theta_f$, $p_{fz} = (E_f^2 - M^2)^{1/2}\cos\theta_f$. The differential cross section can be expressed as

$$d\sigma = \frac{Z^2\alpha^3}{2}\delta(\omega + E_f - E_i)(E_f - M)(E_i - M) \times \frac{p_{f\perp}k_\perp}{|\vec{p}_f|^2|\vec{p}_i|^3}|\xi^{s_f\dagger}(\Sigma_1 + \Sigma_2)\xi^{s_i}|^2 dE_f d\theta_f d\omega d\theta_k, \quad (13)$$

where $\alpha = \frac{e^2}{4\pi}$ is the fine-structure constant. Integrate E_f with the δ function $\delta(\omega + E_f - E_i)$. The incident electron propagates the z axis [$\vec{p}_i = (0, 0, p_{iz})$], therefore

$$d\sigma = \frac{Z^2\alpha^3}{2}(E_f - M)(E_i - M)\frac{p_{f\perp}k_\perp}{|\vec{p}_f|^2|p_{iz}|^3} \times |\xi^{s_f\dagger}(\Sigma_1 + \Sigma_2)\xi^{s_i}|^2 d\omega d\theta_k d\theta_f|_{E_f = E_i - \omega}. \quad (14)$$

The differential cross section of P-V bremsstrahlung is obtained. Equation (15) shows the differential cross section of PW bremsstrahlung (see Appendix B for the specific calculation):

$$d\sigma(PW) = \frac{Z^2\alpha^3}{2\pi}(E_f - M)(E_i - M)\frac{p_{f\perp}k_\perp}{|\vec{p}_f|^2|p_{iz}|^3} \times |W|^2 d\omega d\theta_k d\phi_k d\theta_f|_{E_f = E_i - \omega}. \quad (15)$$

By comparing the forms of two differential cross sections, we notice that there is an additional angular integration in the PW case because there is an angle between the electron and photon emitted in the vertical plane. While for the vortex, it is symmetric about the z axis and this angle has been integrated

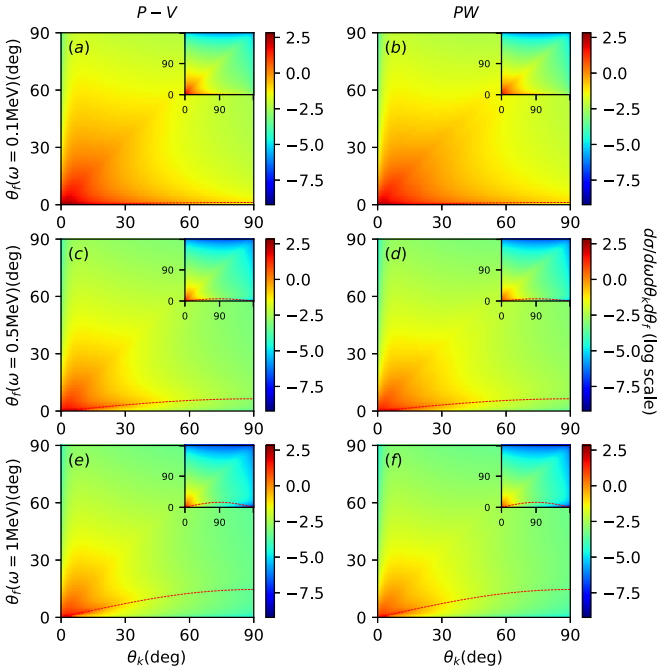

FIG. 2. Opening angles vs cross-section distribution. The first column is the P-V bremsstrahlung case while the second column is the PW case. The incident electron energy is $E_i = 5$ MeV, different rows represent different photon-energy values, l ranges from -20 to $+20$. Red dashed arc curve in each figure is the kinematic transverse momentum constraint curve ($p_{f\perp} = k_\perp$). The distribution of 0–π is shown in the upper-right corner of each figure.

when defining the vortex states. Meanwhile, the P-V case has one more Kronecker symbol, representing the additional angular-momentum restriction.

IV. NUMERICAL RESULTS AND DISCUSSION

The differential cross-section of P-V bremsstrahlung obtained above can be numerically analyzed. Here we focus on the OAM information and the opening angles. In particular, we are interested in how the spin-orbit angular momentum is transferred and distributed.

Averaging over the initial-state spin orientations, summing over the final-state spin orientations, the cross section as a function of the opening angles or emitting angles for outgoing particles is calculated according to Eqs. (14) and (15). The numerical results are shown in Fig. 2, where the incident electron energy is $E_i = 5$ MeV and the outgoing photon energy takes $\omega = 0.1$ MeV, $\omega = 0.5$ MeV and $\omega = 1$ MeV, respectively. Here the l of vortex photon ranges from -20 to $+20$. Comparing between the two cases, we notice that both have identical distributions under all three photon energies. This indicates that the completeness of the P-V bremsstrahlung theory is guaranteed after replacing the final PW states by quantum vortex states.

To analyze the distribution structure under different photon energies, the relationship between electron and photon angles from the perspective of classical kinematics is discussed. In our model, the nucleus is stationary on the z axis,

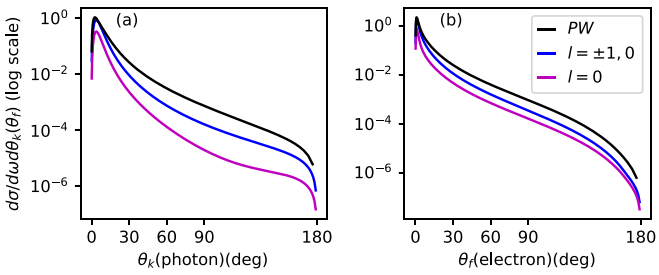

FIG. 3. Angle vs cross-section spectrum of P-V and PW bremsstrahlung. Panel (a) is the photon opening angle spectrum while panel (b) is the electron case. $E_i = 5$ MeV. The magenta and blue lines represent the P-V cases with different l values. Black lines represent the PW case.

the electron collides the nucleus along the z axis. When the photon energy is relatively low, it is close to elastic scattering where the transverse momentum is conserved ($p_{f\perp} = k_\perp$). We obtain the constraint relationship between the electron angle and the photon angle: $p_f \sin\theta_f = k \sin\theta_k$ which can be written as $[(E_i - \omega)^2 - M^2]^{1/2} \sin\theta_f = \omega \sin\theta_k$. Through this constraint relationship and the value of one angle, we can calculate the value corresponding to the other angle, shown as red dashed arc curves in Fig. 2. The distributions in Figs. 2(a) and 2(b) for $\omega = 0.1$ MeV show large cross-section values around this curve. In addition, it seems that their exists a peak where the divergence angles of electron and photon tend to be equal. With the photon energy increasing from 0.1 to 1 MeV, the elastic-scattering condition is no longer well satisfied, the distribution gradually concentrates at smaller angles. Both trends disappear at large photon energies, as seen in Figs. 2(c)–2(f).

Figure 3 shows the more detailed opening angle distribution spectrum of final vortex particles vs photon opening-angle distribution [Fig. 3(a)] and electron opening angle distribution [Fig. 3(b)] (by integrating another angle) in the PW and P-V cases with different l ranges. All six differential cross-section lines reach maximum positions at small angles. With the increase of angles, the differential cross sections decrease gradually. This distribution trend does not change with PW or P-V and different l-ranges of the P-V.

The differential cross section in the P-V case with $l = 0$ is below the PW value. The gap is narrowed when adding the cross sections of three values $l = \pm 1, 0$. This implies that although the PW case does not contain OAM information, it is not a special case of P-V bremsstrahlung with OAM equal to zero. In terms of the cross sections, the result of the P-V scattering tends to converge to the PW case when including more OAM modes. The results numerically prove the completeness of the P-V bremsstrahlung theory again.

In the following, we show how the OAM is allocated among the final vortex particles, which is unknown in the normal PW scattering picture. We take $E_i = 5$ MeV, $\omega = 1$ MeV and sum the spins of outgoing particles but consider the polarization of incident electrons separately. Figure 4 shows the OAM distribution of outgoing vortex photon and electron at different opening angles. When calculating one angle, the other angle is integrated from 0 to π. In general, the cross

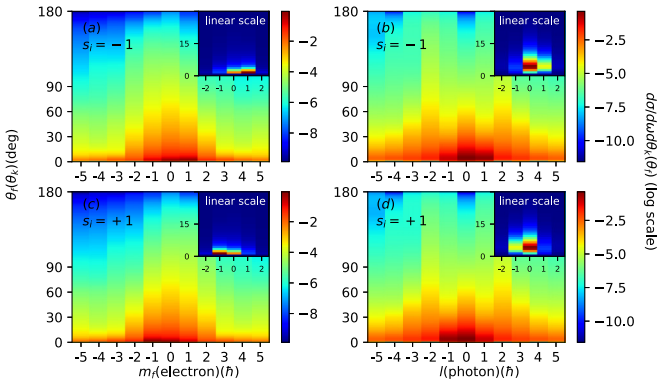

FIG. 4. OAM distribution of P-V bremsstrahlung. Panels (a) and (c) are the outgoing electron OAM m_f and opening angle θ_f vs cross-section distribution, while panels (b) and (d) are the photon case l and θ_k. The other angle is integrated from 0 to π. The polarization of incident electrons is -1 in panels (a) and (b) while the one is $+1$ in panels (c) and (d).

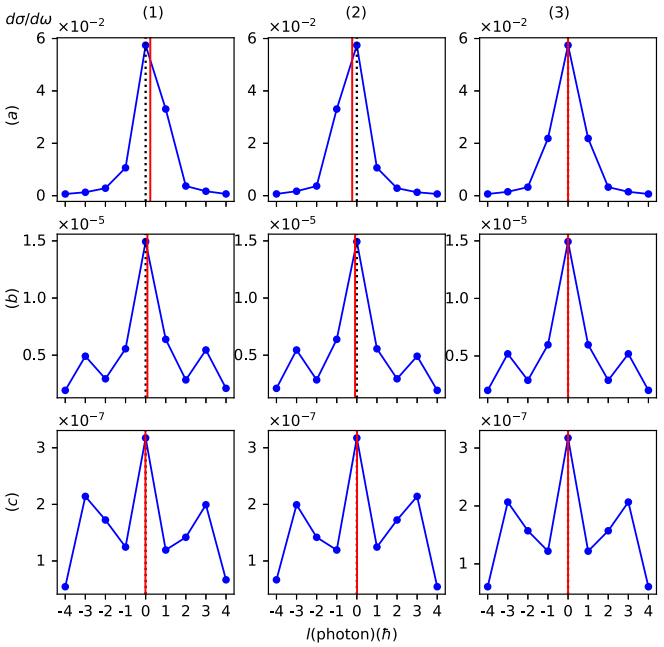

FIG. 5. l distribution over different opening angle ranges. Three rows (a), (b), and (c) are 0°–30°, 60°–90°, and 120°–150°, respectively. Both electron and photon angles are integrated follow the specified range. Three columns (1), (2), and (3) represent incident elections polarization of -1, $+1$, and 0, respectively. Red solid lines mark the average l.

sections of both the vortex electron and photon decrease at larger angles, which is consistent with the results in Fig. 3. The OAM distribution patterns of the electron and photon are very different by comparing Figs. 4(a) with 4(b) and 4(c) with 4(d). The range of l carried by vortex photon is more widely distributed than that of the electron, especially for $\theta_f(\theta_k) > 30°$. At an angle slightly larger than the maximum, the electron m_f distribution presents a Gaussian-like distribution around $m_f = 0$, while the photon l distribution not only shows a peak around $l = 0$, but also at $l = \pm 2$ on both sides. More importantly, it can be found that the polarization of incident electrons mainly offsets the m_f and l distributions. When the initial polarization is -1, m_f and l concentrate at 0 and $+1$ in Figs. 4(a) and 4(b); when the polarization is $+1$, m_f and l concentrate at 0 and -1 in Figs. 4(c) and 4(d). This offset could lead to nonvanishing average OAM values, i.e., the final particles can carry net OAM.

Further relationship between OAM distribution and opening angles is analyzed. We select three angle ranges of 0°–30°, 60°–90°, and 120°–150° to calculate the OAM distribution of photon, as shown in Fig. 5. First, we notice that, at smaller angles 0°–30°, the peak value is located at $l = 0$. When going to larger angles 60°–90° and 120°–150°, secondary peaks appear appear around $l = \pm 3$, which becomes higher upon increasing the angle. Comparing columns (1) and (2) in Fig. 5, the slight asymmetry of the distribution is reflected by the average l value marked by red solid lines in each figure. These offsets discussed in previous section are also represented by red solid lines that deviate from the zero value in the figure, which show a high correlation with the polarization of incident electrons. Average l tends to offset in the opposite direction of electron polarization. These reveal that the l distribution of the differential cross section is highly related to the angle and the incident electron polarization, which could be verified experimentally by the detection of different azimuth angles and the control of different polarization of incident electrons.

It is worth noting that, in combination with Figs. 4 and 5, the OAM distributions under the incident electron polarization of -1 and $+1$ is symmetrical around $l = 0$. Therefore, as shown red solid lines in the third column (3) of Fig. 5, the l is exactly zero after averaging over the initial electron polarization. While spin-to-orbital transfer exists in either case, finite OAM value appears when there is nonzero initial angular-momentum. In this case, the initial electron should be spin polarized.

In normal PW bremsstrahlung, since only SAM is considered, the TAM before and after scattering only calculating the leading order Feynman diagram cannot be well handled [1]. This problem is naturally resolved when the final particles are described by the vortex states. In P-V scattering, the SAM of the initial particles will not only transfer to the SAM of the final particles, but also to the OAM of the final particles. The final TAM consists of SAM and OAM together, and the difference between the initial and final SAMs can be exactly offset by OAM.

Figure 6 shows the numerical results of angular momentum before and after bremsstrahlung at different electron and photon energies at the leading order of the Feynman diagram. All projection numbers of OAM, SAM, and TAM are average values. It can be seen that TAM (only SAM is considered here) of the final states and the initial states in PW bremsstrahlung are not equal. When the photon-energy ratio is relatively low, the TAM difference before and after scattering is close to zero, but the gap increases with the photon energy ratio is larger,

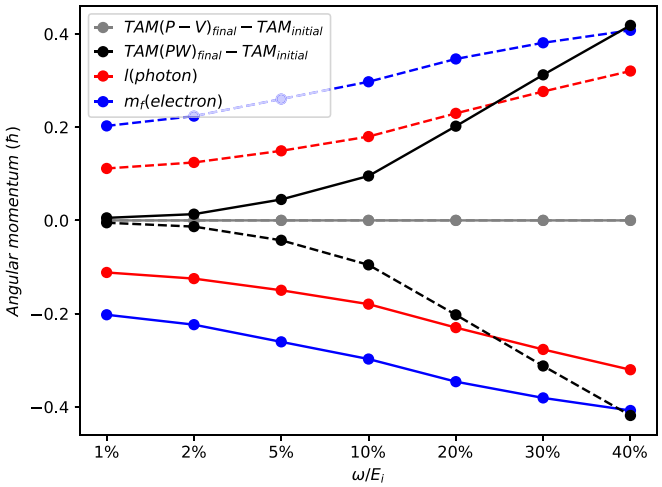

FIG. 6. Numerical results of angular momentum before and after bremsstrahlung. $E_i = 5$ MeV, l ranges from -10 to $+10$. Different color lines represent different angular-momentum quantities marked in figure. The solid lines indicates that the electrons polarization is $+1$, and dashed lines indicate that the polarization of incident electrons is -1.

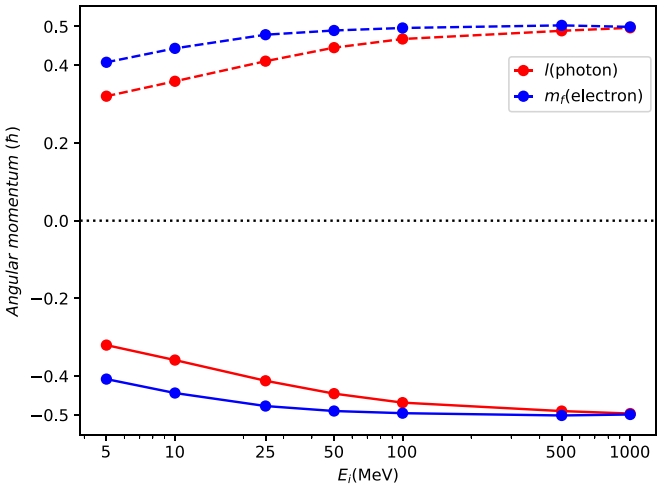

FIG. 7. Numerical results of angular momentum with different incident electron energies. $\omega/E_i = 40\%$, l ranges from -10 to $+10$. Two color lines represent two angular-momentum quantities marked in figure. The solid lines indicates that the electrons polarization is $+1$, and dashed lines indicate that the polarization of incident electrons is -1.

denoted by the two black lines in Fig. 6. When the vortex states are used to describe the final particles, part of SAM is transferred to OAM, and TAM before and after in each spin condition and each photon-energy ratio equals each other in extremely high precision, shown as two overlapping gray lines on the central axis in Fig. 6.

Moreover, Fig. 6 indicates that the OAMs carried by photon and electron are positively correlated to the proportion of photon energy (see two red and two blue lines). All these values are reversed when switching the polarization of the incident electron (solid lines vs dashed lines). When the polarization is averaged, these distributions are smoothed out to zero. Therefore, both the final electron and photon carry zero OAM values if the incident electrons are unpolarized, which means that the OAMs of final particles originate from the polarization of the incident electron rather than the distribution between the final two particles. It reveals the channel through which SAM of the initial electron is transferred to OAMs of the final electron and photon.

The OAM obtained by final photon and electron as a function of the incident electron energy is summarized in Fig. 7, with photon-electron energy ratio fixed at $\omega = 0.40E_i$. We find that the absolute values of l and m_f gradually converge to 0.5 when E_i changes from 5 MeV to 1 GeV. These results indicate that the OAMs transferred to outgoing electron and photon are positively correlated to both the incident electron-energy and photon-energy ratio. The revelation of the physical picture in the highly relativistic regime has enlightenment for the possible experiments in electron accelerator laboratories.

V. CONCLUSION

In this paper, we first used the constructed vortex states wave functions to calculate the differential cross section of P-V bremsstrahlung which the initial electron is described by plane-wave states and the final electron and photon are vortex states in the QED framework. By analyzing the four Kronecker symbols appearing in the cross section, we obtained the relationship between SAM and OAM before and after scattering, which is consistent with the conservation law of total angular momentum. Furthermore, we analyzed the angular distribution characteristics of the final particles by numerically calculating the cross section and comparing it with the classical PW bremsstrahlung. We found that, due to the OAM information carried by the vortex wave functions, it naturally shows the OAM distribution of the final particles, which cannot be revealed by ordinary PW bremsstrahlung. In theory, the final electron and photon can also carry OAM after polarized PW electron scattering. Finally, it is shown that the P-V bremsstrahlung naturally satisfies the conservation law of total angular momentum, and the characteristics that SAM can be transferred to OAM under different photon energy ratios are obtained. These properties related to angular momentum could bring new information for further exploration in various scattering processes in the field of nuclear physics and particle physics.

ACKNOWLEDGMENTS

This work is supported by the National Science Foundation of China (Grants No. 11875307 and No. 11935008), the Strategic Priority Research Program of Chinese Academy of Sciences (Grant No. XDB16010000) and the Ministry of Science and Technology of the People's Republic of China (Grant No. 2018YFA0404803).

APPENDIX A

Some mathematical formulas and specific expressions in the theoretical derivation are shown below.
In a cylindrical coordinate system, e^{-ipx} can be expanded as follows:

$$e^{-ipx} = e^{ip_z z - ip^0 t}\sum_n i^n J_n(p_\perp r)e^{in\theta - in\phi_p}, \tag{A1}$$

$$\cos\phi_p = \frac{p^1}{p_\perp}. \tag{A2}$$

For integer order Bessel functions of the first kind:

$$J_{-n}(x) = (-1)^n J_n(x). \tag{A3}$$

Integration of the twofold Bessel functions:

$$\int dr r J_0(p_\perp r)J_0(q_\perp r) = \frac{1}{p_\perp}\delta(p_\perp - q_\perp), \tag{A4}$$

$$\int dr' r' J_l(k_\perp r')J_{-l}(p_\perp r') = (-1)^l\frac{1}{p_\perp}\delta(p_\perp - k_\perp), \tag{A5}$$

$$\int dr' r' J_{l+1}(k_\perp r')J_{-l-1}(p_\perp r') = (-1)^{l+1}\frac{1}{p_\perp}\delta(p_\perp - k_\perp), \tag{A6}$$

$$\int dr' r' J_{l-1}(k_\perp r')J_{-l+1}(p_\perp r') = (-1)^{l-1}\frac{1}{p_\perp}\delta(p_\perp - k_\perp). \tag{A7}$$

Integration of the triple Bessel functions:

$$\begin{aligned} S_n^m(p,k,q) &= \int dr r J_n(pr)J_{m-n}(qr)J_m(kr) \\ &= \frac{1}{2\pi Aera_{p,q,k}}\cos\left(n\angle(p,k) - (m-n)\angle(k,q)\right), \end{aligned} \tag{A8}$$

where $\angle(a,b)$ represents angle between $\vec{a}$ and $\vec{b}$ and $Aera_{a,b,c}$ represents the area of the triangle formed by a, b, c.
The matrices in Eq. (6) and Eq. (7) are as follows:

$$M_1 = (E_f + M)(E_i + M)\begin{bmatrix} \left(p_z\frac{\lambda k_\perp}{\omega}S_l^0(k_\perp, p_\perp, p_{f\perp}) + p_\perp\left(1-\frac{\lambda k_z}{\omega}\right)S_{l+1}^1\right)\delta_{m_f,-j} & \left(-ip_\perp\frac{\lambda k_\perp}{\omega}S_l^{-1} + ip_z\left(1-\frac{\lambda k_z}{\omega}\right)S_{l+1}^0\right)\delta_{m_f,-j-1} \\ \left(-ip_z\left(1+\frac{\lambda k_z}{\omega}\right)S_{l-1}^0 - ip_\perp\frac{\lambda k_\perp}{\omega}S_l^1\right)\delta_{m_f,-j+1} & \left(-p_\perp\left(1+\frac{\lambda k_z}{\omega}\right)S_{l-1}^{-1} + p_z\frac{\lambda k_\perp}{\omega}S_l^0\right)\delta_{m_f,-j} \end{bmatrix}, \tag{A9}$$

$$M_2 = p_{iz}(E_f + M)(E_p - M)\begin{bmatrix} \frac{\lambda k_\perp}{\omega}S_l^0\delta_{m_f,-j} & i\left(1-\frac{\lambda k_z}{\omega}\right)S_{l+1}^0\delta_{m_f,-j-1} \\ -i\left(1+\frac{\lambda k_z}{\omega}\right)S_{l-1}^0\delta_{m_f,-j+1} & \frac{\lambda k_\perp}{\omega}S_l^0\delta_{m_f,-j} \end{bmatrix}, \tag{A10}$$

$$M_3 = p_{fz}(E_p + M)(E_i + M)\begin{bmatrix} \frac{\lambda k_\perp}{\omega}S_l^0\delta_{m_f,-j} & -i\left(1-\frac{\lambda k_z}{\omega}\right)S_{l+1}^0\delta_{m_f,-j-1} \\ i\left(1+\frac{\lambda k_z}{\omega}\right)S_{l-1}^0\delta_{m_f,-j+1} & \frac{\lambda k_\perp}{\omega}S_l^0\delta_{m_f,-j} \end{bmatrix}, \tag{A11}$$

$$M_4 = p_{iz}p_{fz}\begin{bmatrix} \left(p_z\frac{\lambda k_\perp}{\omega}S_l^0 + p_\perp\left(1-\frac{\lambda k_z}{\omega}\right)S_{l+1}^1\right)\delta_{m_f,-j} & \left(ip_\perp\frac{\lambda k_\perp}{\omega}S_l^{-1} - ip_z\left(1-\frac{\lambda k_z}{\omega}\right)S_{l+1}^0\right)\delta_{m_f,-j-1} \\ \left(ip_z\left(1+\frac{\lambda k_z}{\omega}\right)S_{l-1}^0 + ip_\perp\frac{\lambda k_\perp}{\omega}S_l^1\right)\delta_{m_f,-j+1} & \left(-p_\perp\left(1+\frac{\lambda k_z}{\omega}\right)S_{l-1}^{-1} + p_z\frac{\lambda k_\perp}{\omega}S_l^0\right)\delta_{m_f,-j} \end{bmatrix}, \tag{A12}$$

$$M_5 = -ip_{f\perp}(E_p + M)(E_i + M)\begin{bmatrix} -i\left(1+\frac{\lambda k_z}{\omega}\right)S_{l-1}^0\delta_{m_f,-j} & -\frac{\lambda k_\perp}{\omega}S_l^0\delta_{m_f,-j-1} \\ -\frac{\lambda k_\perp}{\omega}S_l^0\delta_{m_f,-j+1} & i\left(1-\frac{\lambda k_z}{\omega}\right)S_{l+1}^0\delta_{m_f,-j} \end{bmatrix}, \tag{A13}$$

$$M_6 = -ip_{f\perp}p_{iz}\begin{bmatrix} \left(-ip_z\left(1+\frac{\lambda k_z}{\omega}\right)S_{l-1}^0 - ip_\perp\frac{\lambda k_\perp}{\omega}S_l^1\right)\delta_{m_f,-j} & \left(p_\perp\left(1+\frac{\lambda k_z}{\omega}\right)S_{l-1}^{-1} - p_z\frac{\lambda k_\perp}{\omega}S_l^0\right)\delta_{m_f,-j-1} \\ \left(-p_z\frac{\lambda k_\perp}{\omega}S_l^0 - p_\perp\left(1-\frac{\lambda k_z}{\omega}\right)S_{l+1}^1\right)\delta_{m_f,-j+1} & \left(-ip_\perp\frac{\lambda k_\perp}{\omega}S_l^{-1} + ip_z\left(1-\frac{\lambda k_z}{\omega}\right)S_{l+1}^0\right)\delta_{m_f,-j} \end{bmatrix}, \tag{A14}$$

$$M_1' = (E_f + M)(E_i + M)\begin{bmatrix} \left(p_z\frac{\lambda k_\perp}{\omega} + p_\perp\left(1+\frac{\lambda k_z}{\omega}\right)\right)S_l^0(p_\perp, q_\perp, p_{f\perp})\delta_{m_f,-j} & -\left(ip_z\left(1-\frac{\lambda k_z}{\omega}\right) + ip_\perp\frac{\lambda k_\perp}{\omega}\right)S_{l+1}^0\delta_{m_f,-j-1} \\ -\left(ip_\perp\frac{\lambda k_\perp}{\omega} - ip_z\left(1+\frac{\lambda k_z}{\omega}\right)\right)S_{l-1}^0\delta_{m_f,-j+1} & \left(-p_\perp\left(1-\frac{\lambda k_z}{\omega}\right) + p_z\frac{\lambda k_\perp}{\omega}\right)S_l^0\delta_{m_f,-j} \end{bmatrix}, \tag{A15}$$

$$M_2' = p_{iz}(E_f + M)(E_p + M)\begin{bmatrix} \frac{\lambda k_\perp}{\omega}S_l^0\delta_{m_f,-j} & i\left(1-\frac{\lambda k_z}{\omega}\right)S_{l+1}^0\delta_{m_f,-j-1} \\ -i\left(1+\frac{\lambda k_z}{\omega}\right)S_{l-1}^0\delta_{m_f,-j+1} & \frac{\lambda k_\perp}{\omega}S_l^0\delta_{m_f,-j} \end{bmatrix}, \tag{A16}$$

$$M_3' = p_{fz}(E_p - M)(E_i + M)\begin{bmatrix} \frac{\lambda k_\perp}{\omega}S_l^0\delta_{m_f,-j} & -i\left(1-\frac{\lambda k_z}{\omega}\right)S_{l+1}^0\delta_{m_f,-j-1} \\ i\left(1+\frac{\lambda k_z}{\omega}\right)S_{l-1}^0\delta_{m_f,-j+1} & \frac{\lambda k_\perp}{\omega}S_l^0\delta_{m_f,-j} \end{bmatrix}, \tag{A17}$$

$$M_4' = p_{fz}p_{iz}\begin{bmatrix} \left(p_z\frac{\lambda k_\perp}{\omega} + p_\perp\left(1+\frac{\lambda k_z}{\omega}\right)\right)S_l^0(p_\perp, q_\perp, p_{f\perp})\delta_{m_f,-j} & \left(ip_z\left(1-\frac{\lambda k_z}{\omega}\right) + ip_\perp\frac{\lambda k_\perp}{\omega}\right)S_{l+1}^0\delta_{m_f,-j-1} \\ \left(ip_\perp\frac{\lambda k_\perp}{\omega} - ip_z\left(1+\frac{\lambda k_z}{\omega}\right)\right)S_{l-1}^0\delta_{m_f,-j+1} & \left(-p_\perp\left(1-\frac{\lambda k_z}{\omega}\right) + p_z\frac{\lambda k_\perp}{\omega}\right)S_l^0\delta_{m_f,-j} \end{bmatrix}, \tag{A18}$$

$$M_5' = -ip_{f\perp}(E_p - M)(E_i + M)\begin{bmatrix} -i\left(1+\frac{\lambda k_z}{\omega}\right)S_{l-1}^0\delta_{m_f,-j} & -\frac{\lambda k_\perp}{\omega}S_l^0\delta_{m_f,-j-1} \\ -\frac{\lambda k_\perp}{\omega}S_l^0\delta_{m_f,-j+1} & i\left(1-\frac{\lambda k_z}{\omega}\right)S_{l+1}^0\delta_{m_f,-j} \end{bmatrix}, \tag{A19}$$

$$M_6' = -ip_{f\perp}p_{iz}\begin{bmatrix} -\left(ip_\perp\frac{\lambda k_\perp}{\omega} - ip_z\left(1+\frac{\lambda k_z}{\omega}\right)\right)S_{l-1}^0\delta_{m_f,-j} & -\left(-p_\perp\left(1-\frac{\lambda k_z}{\omega}\right) + p_z\frac{\lambda k_\perp}{\omega}\right)S_l^0\delta_{m_f,-j-1} \\ -\left(p_z\frac{\lambda k_\perp}{\omega} + p_\perp\left(1+\frac{\lambda k_z}{\omega}\right)\right)S_l^0\delta_{m_f,-j+1} & -\left(ip_z\left(1-\frac{\lambda k_z}{\omega}\right) + ip_\perp\frac{\lambda k_\perp}{\omega}\right)S_{l+1}^0\delta_{m_f,-j} \end{bmatrix}. \tag{A20}$$

All these matrices Eqs. (A9)–(A20) have the same Kronecker symbols at four locations, combining Eqs. (8) and (9), we have

$$\Sigma_1 + \Sigma_2 = \begin{bmatrix} A\delta_{m_f,-j} & B\delta_{m_f,-j-1} \\ C\delta_{m_f,-j+1} & D\delta_{m_f,-j} \end{bmatrix} \tag{A21}$$

$$= \int dq_\perp q_\perp \frac{1}{(p^2 - M^2)|\vec{q}\,|^2}(C_1 + C_2), \tag{A22}$$

where A, B, C, and D can be obtained by numerical calculation.

APPENDIX B

The S-matrix element for PW bremsstrahlung is

$$\begin{aligned} S_{PW} &= -ie^2\int d^4x d^4y \bar{\psi}_f(x)[\not{A}^*(x)S_F(x-y)\gamma^0 A_0(y) + \gamma^0 A_0(x)S_F(x-y)\not{A}^*(y)]\psi_i(y) \\ &= \frac{iZ\alpha^{\frac{3}{2}}}{4\pi^2\sqrt{\omega E_f E_i}}\delta(E_f + \omega - E_i)\frac{1}{\left|\vec{p}_f + \vec{k} - \vec{p}_i\right|^2}\left[\sqrt{E_f + M}\xi^{s_f^\dagger} \quad -\sqrt{E_f - M}\xi^{s_f^\dagger}\left(\vec{\sigma}\cdot\frac{\vec{p}_f}{|\vec{p}_f|}\right)^\dagger\right] \\ &\times\left[\not{\epsilon}_{\vec{k}}^{*\lambda}\frac{\not{p}_f + \not{k} + M}{2p_f k}\gamma^0 + \gamma^0\frac{\not{p}_i - \not{k} + M}{-2p_i k}\not{\epsilon}_{\vec{k}}^{*\lambda}\right]\begin{bmatrix}\sqrt{E_i + M}\xi^{s_i} \\ \sqrt{E_i - M}\left(\vec{\sigma}\cdot\frac{\vec{p}_i}{|\vec{p}_i|}\right)\xi^{s_i}\end{bmatrix}. \end{aligned} \tag{B1}$$

We define

$$W = \frac{1}{\left|\vec{p}_f + \vec{k} - \vec{p}_i\right|^2}\left[(E_f + M)\xi^{s_f^\dagger} \quad -\xi^{s_f^\dagger}(\vec{\sigma}\cdot\vec{p}_f)^\dagger\right]\left[\not{\epsilon}_{\vec{k}}^{\lambda *}\frac{\not{p}_f + \not{k} + M}{2p_f k}\gamma^0 + \gamma^0\frac{\not{p}_i - \not{k} + M}{-2p_i k}\not{\epsilon}_{\vec{k}}^{\lambda *}\right]\begin{bmatrix}(E_i + M)\xi^{s_i} \\ (\vec{\sigma}\cdot\vec{p}_i)\xi^{s_i}\end{bmatrix}. \tag{B2}$$

The S-matrix element can be written as follows:

$$S_{\rm PW} = \frac{iZ\alpha^{\frac{3}{2}}}{4\pi^2\sqrt{\omega E_f E_i}}\delta(E_f + \omega - E_i)\frac{\sqrt{E_f - M}\sqrt{E_i - M}}{|\vec{p}_f||\vec{p}_i|}W. \tag{B3}$$

The differential cross section is

$$d\sigma(\rm PW) = \frac{|S_{\rm PW}|^2\left(\frac{(2\pi)^3}{V}\right)d^3k d^3p_f}{T\frac{|\vec{v}_i|}{V}} = \delta(E_f + \omega - E_i)\frac{Z^2\alpha^3(E_f - M)(E_i - M)}{4\pi^2\omega E_f|\vec{p}_f|^2|\vec{p}_i|^3}|W|^2 d^3k d^3p_f, \tag{B4}$$

$$d^3k = k_\perp dk_\perp dk_z d\theta_k = \omega^2 d\omega d\Omega_k = \sin\theta_k \omega^2 d\omega d\theta_k d\phi_k, \tag{B5}$$

$$d^3p_f = p_{f\perp} dp_{f\perp} dp_{fz} d\theta_f = \sqrt{E_f^2 - M^2}\sin\theta_f E_f dE_f d\theta_f d\phi_f. \tag{B6}$$

Finally, we have

$$d\sigma(\mathrm{PW}) = \frac{Z^2\alpha^3}{2\pi}(E_f - M)(E_i - M)\frac{p_{f\perp}k_\perp}{|\vec{p}_f|^2|p_{iz}|^3}|W|^2 d\omega d\theta_k d\phi_k d\theta_f|_{E_f = E_i - \omega}. \tag{B7}$$

[1] V. B. Berestetskii, E. M. Lifshitz, and L. P. Pitaevskii, *Quantum Electrodynamics* (Pergamon Press, Oxford, 1982).

[2] L. Allen, M. W. Beijersbergen, R. J. C. Spreeuw, and J. P. Woerdman, Orbital angular momentum of light and the transformation of Laguerre-Gaussian laser modes, Phys. Rev. A **45**, 8185 (1992).

[3] H. He, M. E. J. Friese, N. R. Heckenberg, and H. Rubinsztein-Dunlop, Direct Observation of Transfer of Angular Momentum to Absorptive Particles from a Laser beam with a Phase Singularity, Phys. Rev. Lett. **75**, 826 (1995).

[4] A. T. O'Neil, I. MacVicar, L. Allen, and M. J. Padgett, Intrinsic and Extrinsic Nature of the Orbital Angular Momentum of a Light beam, Phys. Rev. Lett. **88**, 053601 (2002).

[5] M. De Graef, *Introduction to Conventional Transmission Electron Microscopy* (Cambridge University Press, Cambridge, 2003).

[6] W. D. B. C. C. Barry, *Transmission Electron Microscopy* (Springer, New York, 1996).

[7] L. Reimer and H. Kohl, *Transmission Electron Microscopy, Optical Sciences* (Springer Verlag, New York, 2008).

[8] J. Verbeeck, H. Tian, and P. Schattschneider, Production and application of electron vortex beams, Nature (London) **467**, 301 (2010).

[9] M. Uchida and A. Tonomura, Generation of electron beams carrying orbital angular momentum, Nature (London) **464**, 737 (2010).

[10] K. Y. Bliokh and F. Nori, Spatiotemporal vortex beams and angular momentum, Phys. Rev. A **86**, 033824 (2012).

[11] K. Y. Bliokh, M. R. Dennis, and F. Nori, Position, spin, and orbital angular momentum of a relativistic electron, Phys. Rev. A **96**, 023622 (2017).

[12] B. J. McMorran, A. Agrawal, I. M. Anderson, A. A. Herzing, H. J. Lezec, J. J. McClelland, and J. Unguris, Electron vortex beams with high quanta of orbital angular momentum, Science **331**, 192 (2011).

[13] I. P. Ivanov, Colliding particles carrying nonzero orbital angular momentum, Phys. Rev. D **83**, 093001 (2011).

[14] D. Seipt, A. Surzhykov, and S. Fritzsche, Structured x-ray beams from twisted electrons by inverse Compton scattering of laser light, Phys. Rev. A **90**, 012118 (2014).

[15] V. Serbo, I. P. Ivanov, S. Fritzsche, D. Seipt, and A. Surzhykov, Scattering of twisted relativistic electrons by atoms, Phys. Rev. A **92**, 012705 (2015).

[16] M. E. Groshev, V. A. Zaytsev, V. A. Yerokhin, and V. M. Shabaev, Bremsstrahlung from twisted electrons in the field of heavy nuclei, Phys. Rev. A **101**, 012708 (2020).

[17] I. P. Ivanov, Measuring the phase of the scattering amplitude with vortex beams, Phys. Rev. D **85**, 076001 (2012).

[18] I. P. Ivanov, D. Seipt, A. Surzhykov, and S. Fritzsche, Double-slit experiment in momentum space, Europhys. Lett. **115**, 41001 (2016).

[19] I. P. Ivanov, D. Seipt, A. Surzhykov, and S. Fritzsche, Elastic scattering of vortex electrons provides direct access to the Coulomb phase, Phys. Rev. D **94**, 076001 (2016).

[20] D. Karlovets, Probing phase of a scattering amplitude beyond the plane-wave approximation, Europhys. Lett. **116**, 31001 (2016).

[21] D. V. Karlovets, Scattering of wave packets with phases, J. High Energy Phys. 03 (2017) 049.

[22] I. P. Ivanov, High-energy physics with particles carrying non-zero orbital angular momentum, Few-Body Syst. **53**, 167 (2012).

[23] I. P. Ivanov, Probing the phase of the elastic pp scattering amplitude with vortex proton beams, AIP Conf. Proc. **1523**, 128 (2013).

[24] U. D. Jentschura and V. G. Serbo, Generation of High-energy Photons with Large Orbital Angular Momentum by Compton Backscattering, Phys. Rev. Lett. **106**, 013001 (2011).

[25] U. D. Jentschura and V. G. Serbo, Compton upconversion of twisted photons: Backscattering of particles with non-planar wave functions, Eur. Phys. J. C **71**, 1571 (2011).

[26] I. P. Ivanov and V. G. Serbo, Scattering of twisted particles: Extension to wave packets and orbital helicity, Phys. Rev. A **84**, 033804 (2011).

[27] I. P. Ivanov, Creation of two vortex-entangled beams in a vortex-beam collision with a plane wave, Phys. Rev. A **85**, 033813 (2012).

[28] J. A. Sherwin, Two-photon annihilation of twisted positrons, Phys. Rev. A **98**, 042108 (2018).

[29] D. Karlovets, Relativistic vortex electrons: Paraxial versus nonparaxial regimes, Phys. Rev. A **98**, 012137 (2018).

[30] D. Karlovets, Dynamical enhancement of nonparaxial effects in the electromagnetic field of a vortex electron, Phys. Rev. A **99**, 043824 (2019).

[31] D. V. Karlovets, G. L. Kotkin, V. G. Serbo, and A. Surzhykov, Scattering of twisted electron wave packets by atoms in the Born approximation, Phys. Rev. A **95**, 032703 (2017).

[32] D. V. Karlovets and V. G. Serbo, Effects of the transverse coherence length in relativistic collisions, Phys. Rev. D **101**, 076009 (2020).

[33] D. V. Karlovets and A. M. Pupasov-Maksimov, Nonlinear quantum effects in electromagnetic radiation of a vortex electron, Phys. Rev. A **103**, 012214 (2021).

[34] I. P. Ivanov, V. G. Serbo, and V. A. Zaytsev, Quantum calculation of the Vavilov-Cherenkov radiation by twisted electrons, Phys. Rev. A **93**, 053825 (2016).

[35] G. Guzzinati, P. Schattschneider, K. Y. Bliokh, F. Nori, and J. Verbeeck, Observation of the Larmor and Gouy Rotations with Electron Vortex Beams, Phys. Rev. Lett. **110**, 093601 (2013).

[36] K. Y. Bliokh, P. Schattschneider, J. Verbeeck, and F. Nori, Electron Vortex Beams in a Magnetic Field: A New Twist on Landau Levels and Aharonov-Bohm States, Phys. Rev. X **2**, 041011 (2012).

[37] A. Pupasov-Maksimov and D. Karlovets, SmithPurcell radiation of a vortex electron, New J. Phys. **23**, 043011 (2021).

[38] P. Schattschneider, Th. Schachinger, M. Stöger-Pollach, S. Löffler, A. Steiger-Thirsfeld, K. Y. Bliokh, and F. Nori, Imaging the dynamics of free-electron Landau states, Nat. Commun. **5**, 4586 (2014).

[39] Z. Bu, L. Ji, S. Lei, H. Hu, X. Zhang, and B. Shen, Twisted Breit-Wheeler electron-positron pair creation via vortex gamma photons, Phys. Rev. Research **3**, 043159 (2021).

[40] P. O. Kazinski and V. A. Ryakin, Radiation of twisted photons in elliptic undulators, Russ. Phys. J. **64**, 717 (2021).

[41] O. V. Bogdanov, P. O. Kazinski, P. S. Korolev, and G. Y. Lazarenko, Generation of hard twisted photons by charged particles in cholesteric liquid crystals, Phys. Rev. E **104**, 024701 (2021).

[42] J. Harris, V. Grillo, E. Mafakheri, G. C. Gazzadi, S. Frabboni, R. W. Boyd, and E. Karimi, Structured quantum waves, Nat. Phys. **11**, 629 (2015).